Eur. Phys. J. D (2022) 76:214
https://doi.org/10.1140/epjd/s10053-022-00539-8

THE EUROPEAN PHYSICAL JOURNAL D

Regular Article – Plasma Physics

Ion energy distribution of plasma ions of a hollow cathode discharge in Ar + N_2 and Ar + O_2 gas mixtures

Rainer Hippler[1,2,a], Martin Cada[1], and Zdenek Hubicka[1]

[1] Institute of Physics, Czech Academy of Sciences, Na Slovance 2, 18221 Prague, Czech Republic
[2] Institut für Physik, Universität Greifswald, Felix-Hausdorff-Str. 6, 17489 Greifswald, Germany

Received 19 September 2022 / Accepted 25 October 2022 / Published online 9 November 2022
© The Author(s) 2022

Abstract. A hollow cathode discharge with a Ti cathode and a positively biased ring anode was operated in Ar + N_2 or Ar + O_2 gas mixtures. The energy distribution of plasma ions is investigated with the help of energy-resolved mass spectrometry. Singly and doubly charged Ar^+ and Ar^{2+} ions and molecular N_2^+ or O_2^+ ions are the most abundant ionic species. The kinetic energy of all plasma ions is enhanced by a positive anode voltage.

1 Introduction

Hollow cathode (HC) discharges are frequently used in many applications, e.g., in atomic spectroscopy, laser technology, as UV generators, and for deposition of thin solid films [1–11]. Typical HCs are made from a cylindrical tube which is open on one or both ends. The discharge is sustained by electrons which undergo a pendulum motion inside the HC [2,12–15]. HC discharges are often operated without a dedicated anode and instead use the walls of the vacuum chamber for this purpose [16,17]. To stabilize the HC discharge, an extra ring anode was recently implemented [18,19]. A biased ring anode offers the additional benefit of controlling the plasma potential outside the HC and the kinetic energy of plasma ions impinging on a substrate [20].

In this communication, we investigate a HC discharge with positively biased anode in a reactive gas environment. Ar + N_2 and Ar + O_2 gas mixtures are employed, and the energy distribution of several plasma ions is investigated.

2 Experiment

A hollow cathode (HC) made from titanium rod (purity 99.95%, length 40 mm, outer diameter 12 mm, inner diameter of 5 mm) is mounted inside a vacuum chamber (Fig. 1) [20]. The HC tube is open on one end and connected to a water-cooling jacket (holder) on the other end. Argon gas is admitted to the hollow cathode through a ceramic gas pipe connected to its back side with a gas flow controller. Typical argon flow rates during HC operation are in the range of 40–280 sccm. N_2 (purity 99.995%) or O_2 gas (purity 99.995%) is admitted directly to the vacuum chamber using a second gas flow controller at typical gas flow rates of 10 sccm. The gas pressure in the vacuum chamber was maintained at 2.1 Pa. The gas pressure inside the nozzle is much larger, however, and, for an Ar gas flow rate of 140 sccm, in the range of 50 Pa [9].

A ring anode made from a DN 63 CF copper gasket (inner diameter 63 mm, outer diameter 82 mm, thickness 2 mm) is mounted at a distance of 100 mm from the cathode. The hollow cathode is powered by a DC power supply (Advanced Energy MDX–500) operated in current regulation mode with a typical discharge current of 0.5 A. The anode is powered by a regulated laboratory DC voltage supply (Manson HCS-3204) with a maximal output voltage of 60 V.

Energy-resolved mass spectrometry is performed with a commercial Hiden EQP 1000 mass/energy analyzer (Hiden Analytical Ltd., UK) [21,22]. The instrument is mounted opposite to the hollow cathode and the anode at a distance of 120 mm from the anode (Fig. 1).

3 Results and discussion

Typical ion mass spectra are displayed in Fig. 2 for a HC discharge operated in Ar + N_2 and Ar + O_2 gas mixtures with an Ar gas flow rate of 80 sccm, a reactive gas (N_2, O_2) flow rate of 10 sccm, a gas pressure of 1.05 Pa, and a discharge current of 0.5 A. The

Guest editors: Jose L. Lopez, Michael Brunger, Holger Kersten.

[a] e-mail: hippler@physik.uni-greifswald.de (corresponding author)

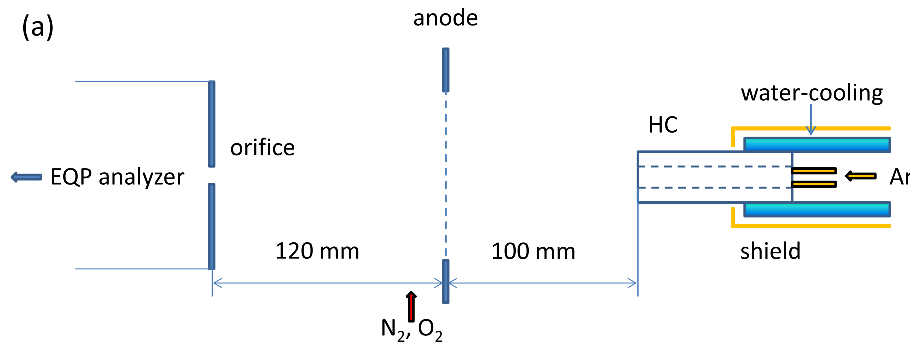

Fig. 1 Experimental set-up with hollow cathode, and orifice of EQP analyzer. Gas inlet positions for Ar and N_2 or O_2 are indicated (schematic)

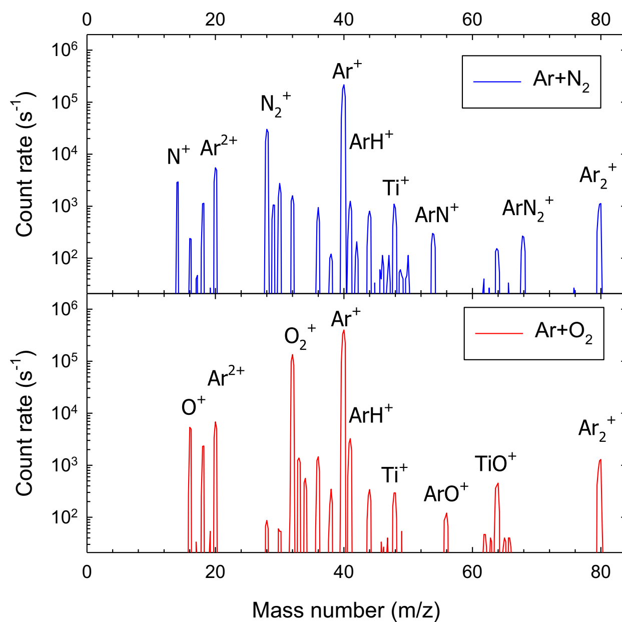

Fig. 2 Mass spectrum **a** Ar + N_2 and **b** Ar + O_2 gas mixture. Anode voltage + 60 V. Ar gas flow rate 80 sccm, reactive gas (N_2 or O_2) gas flow rate 10 sccm, gas pressure 1.05 Pa, discharge current 0.50 A. Detected ion energy 45 eV

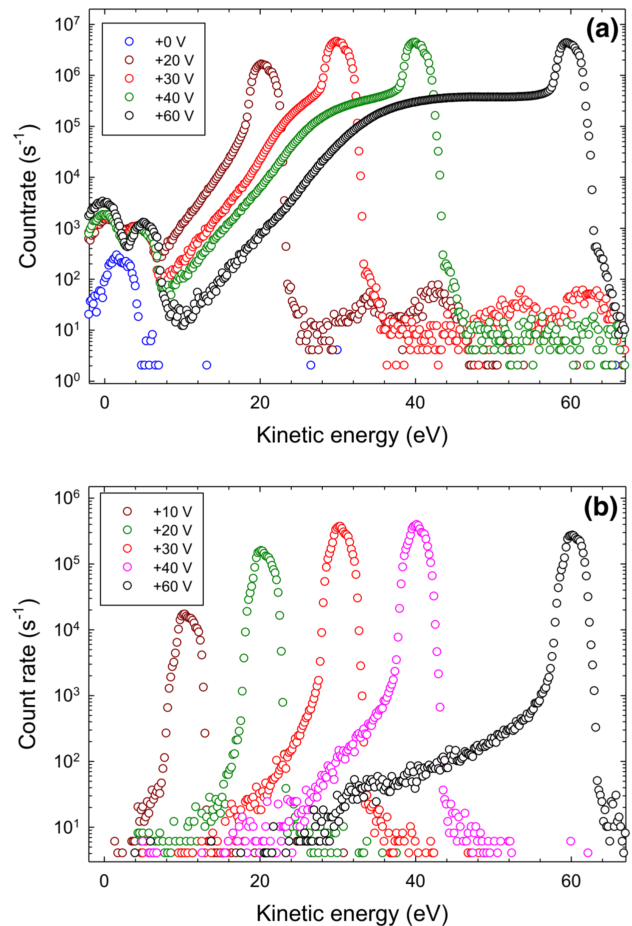

Fig. 3 Ion energy distribution of **a** Ar^+ (○) and **b** Ti^+ (▽) ions for a hollow cathode discharge with different anode bias in pure Ar. Ar gas flow rate 160 sccm, gas pressure 1.7 Pa, discharge current 0.5 A

anode voltage was set to + 60 V. The kinetic energy of detected ions was set to 45 eV which, as we shall see below, is smaller than the value where the maximum ion intensity occurs. The spectra are dominated by singly charged Ar^+ ($m/z = 40$), doubly charged Ar^{2+} ($m/z = 20$), and molecular N_2^+ ($m/z = 28$) or O_2^+ ($m/z = 32$) ions (m and z are mass and charge number, respectively). Also present are singly charged Ti^+ ($m/z = 48$), N^+ ($m/z = 14$) or O^+ ($m/z = 16$), and molecular Ar_2^+ ($m/z = 80$) ions. In addition, we find a significant number of other molecular ions. Molecular ArN^+ ($m/z = 54$) and ArN_2^+ ($m/z = 68$) or ArO^+ ($m/z = 56$) and TiO^+ ($m/z = 64$) ions are produced with the Ar + N_2 or Ar + O_2 gas mixture, respectively.

Ion energy distributions of singly charged Ar^+ and Ti^+ ions measured in pure Ar gas with different anode bias are displayed in Fig. 3. Measured energy distributions shift to higher energies with applied positive anode voltage. The intensity maximum (peak) of the distributions occurs at a kinetic energy close to $E = e_0 V_a$, where e_0 is the elementary charge and V_a is the applied anode voltage. Ar^+ ions show a pronounced low-energy tail extending down to lower kinetic energy

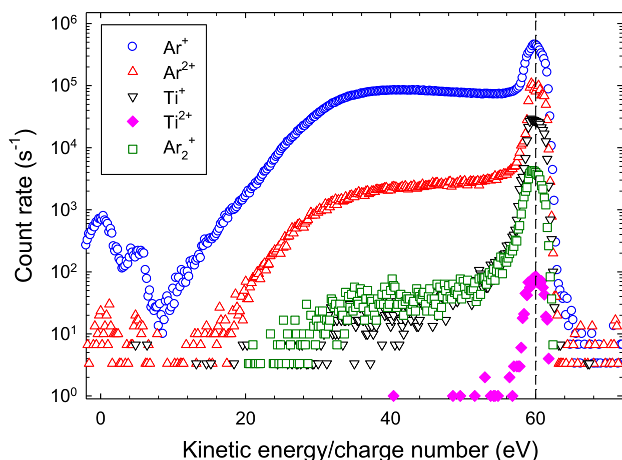

Fig. 4 Ion energy distribution of Ar^+ (○), Ar^{2+} (△), Ti^+ (▽), Ti^{2+} (⧫), and Ar_2^+ (□) ions for a hollow cathode discharge with a positively biased anode (+ 60 V) in pure Ar. Ar gas flow rate 120 sccm, gas pressure 2.1 Pa, discharge current 0.5 A. Vertical dashed line (+ 60 eV) to guide the eye only

which is largely absent for Ti^+ ions. The low-energy tail is caused by the $Ar^+ + Ar \rightarrow Ar + Ar^+$ resonant charge transfer collision which produces a slow Ar^+ ion. The final kinetic energy of this ion is then determined by the plasma potential where the slow ion is produced. Ti^+ ions do not undergo sufficient resonant charge transfer collisions since, for the corresponding $Ti^+ + Ti \rightarrow Ti + Ti^+$ reaction, the Ti density is too small.

Figure 4 compares ion energy distributions of singly charged Ar^+, Ti^+, and Ar_2^+ and doubly charged Ar^{2+} and Ti^{2+} ions plotted versus reduced energy $\tilde{E} = E/z$, where E is the kinetic energy divided by the charge number z. Similar results have been published before [20]. Singly and doubly charged argon ions show a pronounced low-energy tail which presumably is caused by resonant charge changing collisions, e.g., $Ar^{z+} + Ar \rightarrow Ar + Ar^{z+}$. In comparison, the low-energy tail is less pronounced for Ar^{2+} compared to Ar^+ ions. The difference is explained by the smaller resonant charge transfer cross section of Ar^{2+} compared to Ar^+ ions [22–24]. The low-energy tail is much less pronounced for Ti^+, Ti^{2+}, and Ar_2^+ ions. The small intensity of Ti^{2+} ions is not understood yet.

3.1 Ar + N_2

Ion energy distributions of singly charged Ar^+, Ti^+, and N^+ and doubly charged Ar^{2+} and Ti^{2+} ions of a HC discharge in Ar + N_2 are compared in Fig. 5a. Ar^+ ions constitute the dominant mono-atomic ion species, followed by N^+, Ti^+, and Ar^{2+} ions. Ti^{2+} ions are the least abundant of the investigated species. We want to emphasize that no mass-dependent calibration was applied when comparing different ions. A mass-dependent sensitivity of a similar instrument was investigated by Welzel and Ellmer, and no mass dependence was observed in the mass range $m/z > 20$ [25].

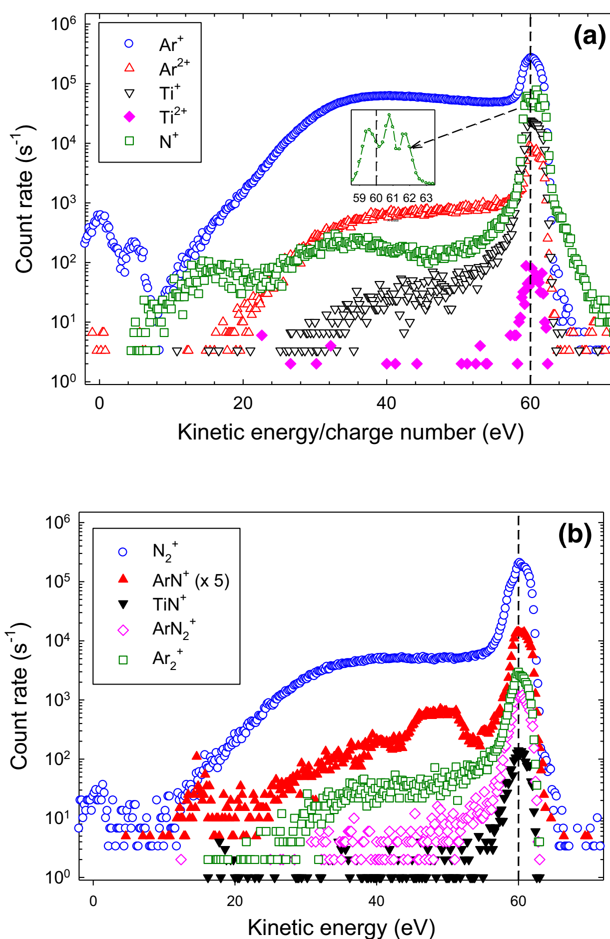

Fig. 5 Ion energy distribution of **a** Ar^+ (○), Ar^{2+} (△), Ti^+ (▽), Ti^{2+} (⧫), and N^+ ions and **b** N_2^+ (○), ArN^+ (▲), TiN^+ (▼), ArN_2^+ (◇) and Ar_2^+ (□) ions for a hollow cathode discharge with a positively biased anode (+ 60 V) in an Ar + N_2 gas mixture. Ar gas flow 120 sccm, N_2 gas flow 10 sccm, gas pressure 2.1 Pa. The inset shows the N^+ intensity around 60 eV. Vertical dashed line (+ 60 eV) to guide the eye only

Ar^+ and Ar^{2+} ions again display a pronounced and monotonously declining low-energy tail. N^+ ions show a complicated low-energy tail structure with two broad humps near 15 eV and 33 eV which may result from in-flight dissociation of N-containing molecules. In addition, N^+ ions show a pronounced high-energy tail extending to larger energies beyond 70 eV. As shown by the inset, the main N^+ peak around 60 eV splits into 3 sub-peaks with energies of 59.5 eV, 60.8 eV, and 61.6 eV whose origin is not known.

Figure 5b displays ion energy distributions of N_2^+, ArN^+, ArN_2^+, TiN^+, and Ar_2^+ molecular ions. The N_2^+ ion intensity is comparable to Ar^+. Ar_2^+, ArN^+, and ArN_2^+ ions are of a comparable intensity. Also observed are TiN^+ ions, albeit with small intensity. The extracted TiN^+/Ti^+ ratio is small and amounts to about 7×10^{-4}. The broad structure at ≈ 48 eV

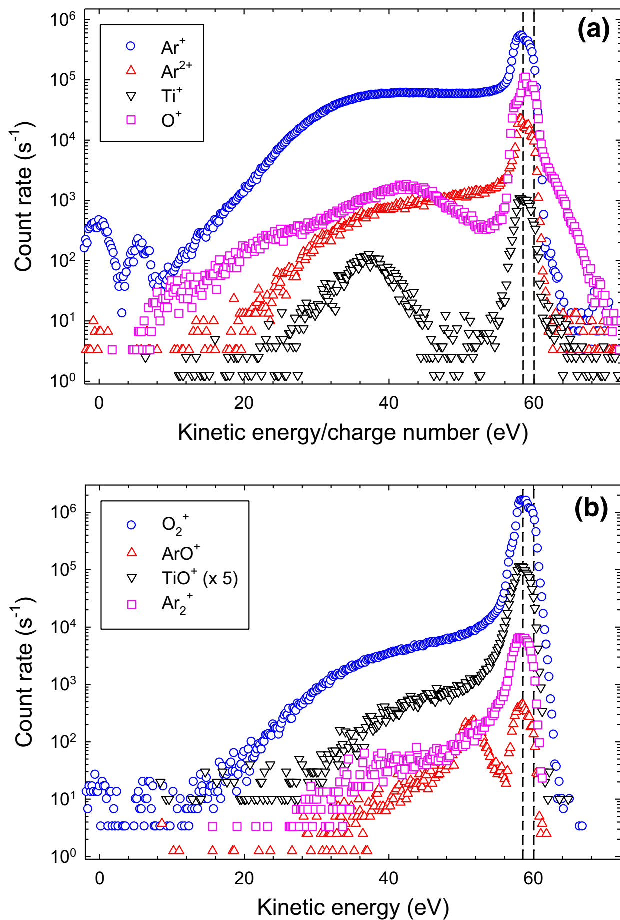

Fig. 6 Ion energy distribution of **a** Ar^+ (○), Ar^{2+} (△), Ti^+ (▽), and O^+ (□) ions and **b** O_2^+ (○), ArO^+ (△), TiO^+ (▽), and Ar_2^+ (□) ions for a hollow cathode discharge with a positively biased anode (+ 60 V) in an Ar + O_2 gas mixture. Ar gas flow 120 sccm, O_2 gas flow 10 sccm, gas pressure 2.1 Pa. Vertical dashed line (+ 60 eV) to guide the eye only

observed for ArN^+ ions is presumably due to in-flight dissociation of ArN_2^+ ions whereby the kinetic energy is shared between the product ArN^+ ion and N atom according to the mass ratio.

3.2 Ar + O_2

Ion energy distributions of singly charged Ar^+, Ti^+, and O^+ and doubly charged Ar^{2+} ions of a HC discharge in Ar + O_2 are compared in Fig. 6. Ar^+ ions are the most abundant atomic species followed by O^+ and Ar^{2+} ions. Ti^+ are the least abundant of the investigated atomic ion species. Molecular ions are compared in Fig. 6b. Molecular O_2^+ is the dominant ion species with a 1.5× larger intensity compared to Ar^+, followed by TiO^+, and Ar^{2+} ions. The extracted TiO^+/Ti^+ ratio is rather large and about 17. Also observed are ArO^+ ions which have the smallest intensity of the investigated molecular species. Ti^{2+} ions were not investigated due to a too small intensity. The energetic position of the ions is about 58.5 eV and, hence 1.5 eV lower than

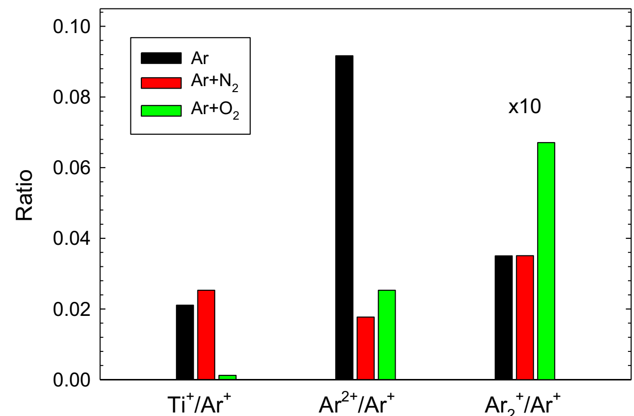

Fig. 7 Energy-integrated Ti^+/Ar^+, Ar^{2+}/Ar^+, and Ar_2^+/Ar^+ ratio for a HC discharge in Ar, Ar + N_2, and Ar + O_2 gas mixtures. Anode voltage + 60 V. Discharge current 0.50 A. Ar gas flow 120 sccm, Ar gas pressure 2.1 Pa. N_2 or O_2 gas flow 10 sccm

for the Ar or Ar + N_2 gas mixtures. We attribute this small albeit significant difference to the existence of negative ions in the plasma which reduces the plasma potential.

In addition to the main peak at 58.5 eV, the energy distributions of O^+, Ti^+, and ArO^+ display pronounced low-energy peaks at 42 eV, 37 eV, and 51 eV, respectively. It appears likely that these peak originate from in-flight dissociation of larger molecular ions similar to the peak observed for ArN^+ ions (see above). For example, the peak at 37 eV observed for Ti^+ ions could arise from dissociation of TiO_2^+ ions, i.e., $TiO_2^+ \rightarrow Ti^+ + O_2$. The pronounced high-energy tail above 60 eV observed for O^+ ions could originate from dissociate ionization of O_2 molecules via a repulsive intermediate state, i.e., $e^- + O_2 \rightarrow O_2^{+*} + 2\, e^-$ followed by $O_2^{+*} \rightarrow O^+ + O$.

3.3 Ion Ratios

Measured Ti^+/Ar^+, Ar^{2+}/Ar^+, and Ar_2^+/Ar^+ ion ratios derived from the energy integrated ion energy distributions are displayed in Fig. 7. Positively charged ions are produced in some distance from the negatively biased cathode. The main process for Ar^+, Ti^+, and Ar^{2+} ion formation is ionization by electron impact [26]. The dominant loss mechanism is via diffusion and the subsequent recombination on surrounding surfaces. Under equilibrium conditions, the corresponding reaction rates are equal and the ion density n_+ is obtained from

$$k_+ n_e n_a = \frac{D_+}{\Lambda^2} n_+, \tag{1}$$

where the left and the right sides of the eqnarray correspond to the formation rate and to the loss by diffusion. k_+ and k_{2+} are rate coefficients for single ionization and double ionization, respectively, n_e and n_a are electron and atom density, respectively, D is the diffusion

constant, L is the length of the plasma column, and $\Lambda = L/\pi$. Assuming equal diffusion constants for Ar^+ and Ar^{2+} ions, we obtain

$$\frac{n_{2+}}{n_+} = \frac{k_{2+}}{k_+}. \quad (2)$$

The observed Ar^{2+}/Ar^+ ion ratio is about 10% for Ar, in fair agreement with more recent observations [26], but considerably smaller (about 2%) for Ar + N_2 and Ar + O_2 gas mixtures. The ratio is quite large considering the plasma conditions which are characterized by a small electron temperature of 0.8 eV only [20] which is typical for DC and pulsed HC discharges [15,27].

Semi-empirical cross sections for single and multiple ionization of argon atoms by electron impact are available from Deutsch et al. [28–31]. A simple estimate shows that formation of doubly ionized Ar^{2+} ions with such low-electron electrons is rather unlikely. Secondary electrons are produced inside the plasma region but also via ion bombardment at the cathode's surface. The subsequently acceleration of the latter electrons in the cathode sheath yields energetic electrons which attain rather large kinetic energies corresponding to the cathode fall potential, i.e., electron energies of several 100 eV. Ionization by energetic electrons, hence, can produce both singly and doubly charged ions. Calculated Ar^{2+}/Ar^+ ratios based on the available semi-empirical cross sections of Deutsch et al. [28–30] yield 5% and 9% at electron energies of 100 eV and 300 eV, respectively, which are in reasonable agreement with the observed ratio. The small Ar^{2+}/Ar^+ ratio in Ar + N_2 or Ar + O_2 is presumably caused by additional Ar^{2+} loss processes, for example, charge changing or rearrangement reactions with N_2 or O_2 molecules, e.g., [32]

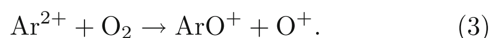

$$Ar^{2+} + O_2 \rightarrow ArO^+ + O^+. \quad (3)$$

The observed Ti^+/Ar^+ ratio is about 2% for Ar and Ar + N_2 and one order of magnitude smaller (about 2×10^{-3}) for the Ar + O_2 gas mixture. Ti^+ ions are produced by a two-step process, i.e., via sputtering of neutral Ti atoms inside the HC and the subsequent ionization by electron impact in the plasma region between cathode and anode. Cross sections and rate coefficients for electron impact ionization of Ti compared to ionization of Ar are much larger at low energies which is due to the lower ionization energy of Ti (6.83 eV [33]) compared to Ar (15.76 eV). Ionization by low-energy electrons, hence, cannot explain the small Ti^+/Ar^+ ratio. At larger electron energies of several 100 eV, the rate coefficients for ionization of Ar and Ti by electron impact are much larger and about equal [34]. Assuming ionization by high-energy electrons as the dominant ionization mechanism and about equal diffusion coefficients for Ar^+ and Ti^+, we have

$$\frac{n_+^{Ti}}{n_+^{Ar}} \approx \frac{n_a^{Ti}}{n_a^{Ar}}. \quad (4)$$

The observed small Ti^+/Ar^+ ratio presumably reflects the much smaller atom density of sputtered Ti atoms compared to Ar atoms. The even smaller Ti^+/Ar^+ ratio observed for the Ar + O_2 gas mixture is readily explained by the additional formation of TiO^+ ions resulting in a strong reduction of the Ti^+ intensity.

Formation of Ar_2^+ ions is more complicated. Most likely are gas phase processes, in particular, (i) three-body reactions of Ar^+ ions with two neutral argon atoms, $Ar^+ + Ar + Ar \rightarrow Ar_2^+ + Ar$, (ii) associative ionization of two metastable Ar_m atoms, $Ar_m + Ar_m \rightarrow Ar_2^+ + e^-$, and (iii) associative ionization of highly excited Ar^{**} with neutral Ar atoms, $Ar^{**} + Ar \rightarrow Ar_2^+ + e^-$ [21,26]. The here observed ratios are 3.5×10^{-3} for Ar and Ar + N_2 gas mixtures and 6.7×10^{-3} for Ar + O_2. Larger ratios were observed by Bogaerts and Gijbels for a dc glow discharge at a gas pressure of 75 Pa where due to the much larger gas pressure (density) the 3-body reaction process is more likely [26].

4 Conclusions

Ion energy distribution measurements have been taken for a hollow cathode discharge in reactive Ar + N_2 and Ar + O_2 gas mixtures. The discharge is operated with a positively biased anode which enhances the plasma potential and, hence, the kinetic energy of plasma ions. For an anode bias voltage of +60 V, the measured ion energy distributions peak at $E = 60$ eV for Ar and Ar + N_2 gas mixtures and at 58.5 eV for Ar + O_2. The difference is attributed to the presence of negative ions in the Ar + O_2 discharge. Ar^+ and Ar^{2+} ions additionally display a pronounced low-energy tail which we attribute to resonant charge exchange processes. N^+ and O^+ ions show more complicated energy distributions including a pronounced high-energy tail which may reflect the formation via intermediate N_2^{+*} or O_2^{+*} repulsive states. Formation of molecular Ar_2^+ and of TiN^+, ArN^+, and ArN_2^+ ions or TiO^+ and ArO^+ ions with the Ar + N_2 or Ar + O_2 gas mixtures are observed. There is a huge difference between the TiN^+/Ti^+ and TiO^+/Ti^+ ratios. The extracted TiN^+/Ti^+ and TiO^+/Ti^+ ratios are about 7×10^{-4} and 17, respectively, and thus rather different. It may reflect the different reaction enthalpies during the collisions of, e.g., Ti^+ ions with N_2 or O_2 molecules. The Ar^{2+}/Ar^+ ion ratio is larger than expected for a discharge with an electron temperature of typically 0.8 eV. It is concluded that high energy electrons which orginate from the negatively biased cathode are responsible for the comparatively large Ar^{2+}/Ar^+ ratio of several percent.

Acknowledgements The work was partly supported by Project No. 21-04477S of the Czech Science Foundation and

Project No. SOLID21-CZ.02.1.01/0.0/0.0/16_019/0000760 of the Operational Programme Research, Development and Education financed by European Structural and Investment Funds and the Czech Ministry of Education, Youth and Sports.

Author contributions

All authors contributed equally to the work.

Funding Information Open Access funding enabled and organized by Projekt DEAL.

Data Availability Statement This manuscript has no associated data or the data will not be deposited. [Authors' comment: Data will be made available upon reasonable request.]

Open Access This article is licensed under a Creative Commons Attribution 4.0 International License, which permits use, sharing, adaptation, distribution and reproduction in any medium or format, as long as you give appropriate credit to the original author(s) and the source, provide a link to the Creative Commons licence, and indicate if changes were made. The images or other third party material in this article are included in the article's Creative Commons licence, unless indicated otherwise in a credit line to the material. If material is not included in the article's Creative Commons licence and your intended use is not permitted by statutory regulation or exceeds the permitted use, you will need to obtain permission directly from the copyright holder. To view a copy of this licence, visit http://creativecommons.org/licenses/by/4.0/.

References

1. F. Paschen, Bohrs Heliumlinien. Ann. Phys. IV **50**, 901 (1916). https://doi.org/10.1002/andp.19163551603
2. G.J.M. Hagelaar, D.B. Mihailova, J. van Dijk, Analytical model of a longitudinal hollow cathode discharge. J. Phys. D: Appl. Phys. **43**, 465204 (2010). https://doi.org/10.1088/0022-3727/43/46/465204
3. D.W. Duquette, J.E. Lawler, Radiative lifetimes in Nb I. Phys. Rev. A **26**, 330 (1982). https://doi.org/10.1103/PhysRevA.26.330
4. D. Ishikawa, S. Hasegawa, Development of removable hollow cathode discharge apparatus for sputtering solid metals. J. Spectrosc. **2019**, 7491671 (2019). https://doi.org/10.1155/2019/7491671
5. K. Ishii, High rate low kinetic energy gas flow sputtering system. J. Vac. Sci. Technol. A **7**, 256 (1989). https://doi.org/10.1116/1.576129
6. H. Koch, L.J. Friedrich, V. Hinkel, F. Ludwig, B. Politt, T. Schurig, Hollow cathode discharge sputtering device for uniform large area thin film deposition. J. Vac. Sci. Technol. A **9**, 2374 (1991). https://doi.org/10.1116/1.577279
7. Z. Hubicka, M. Cada, P. Adamek, P. Virostko, J. Olejnicek, A. Deyneka, L. Jastrabik, K. Jurek, G. Suchaneck, M. Guenther, G. Gerlach, P. Bohac, Investigation of the RF pulse modulated plasma jet system during the deposition of $PbZr_xTi_{1-x}O_3$ thin films on polymer substrates. Surf. Coat. Technol. **200**, 940 (2005). https://doi.org/10.1016/j.surfcoat.2005.02.041
8. Z. Hubicka, J. Olejnicek, M. Cada, P. Virostko, H. Sichova, A. Deyneka, L. Jastrabik, D. Chvostova, M. Sicha, $Ba_xSr_{1-x}TiO_3$ thin films deposited by RF hollow cathode plasma jet technique. Ferroelectrics **317**, 1 (2005). https://doi.org/10.1116/1.57129
9. Z. Hubicka, Hollow cathodes and plasma jets for thin film deposition, in *Low Temperature Plasmas*, vol. 2, ed. by R. Hippler, H. Kersten, M. Schmidt, K.H. Schoenbach (Wiley-VCH, Weinheim, 2008), p.715
10. A. Lunk, Der Hohlkatodenbogen als Plasmaquelle in der Beschichtungstechnik, Ernst Moritz-Arndt-Universität Greifswald, Ph.D. thesis (1985)
11. A. Lunk, Plasma activated physical vapour deposition by hollow cathode arc. Vacuum **41**, 1965 (1990). https://doi.org/10.1016/0042-207X(90)94146-H
12. V.I. Kolobov, L.D. Tsendin, Analytic model of the hollow cathode effect. Plasma Sources Sci. Technol. **4**, 551 (1995). https://doi.org/10.1088/0963-0252/4/4/006
13. J.P. Boeuf, L.C. Pitchford, Field reversal in the negative glow of a DC glow discharge. J. Phys. D Appl. Phys. **28**, 2083 (1995). https://doi.org/10.1088/0022-3727/28/10/013
14. C.J. Timmermans, A. Lunk, D.C. Schram, The rotation of ions and neutrals in a cylindrical magnetized hollow cathode argon arc. Beitr. Plasmaphys. **21**, 178 (1981)
15. M. Tichy, Z. Hubicka, M. Sicha, M. Cada, J. Olejnicek, O. Churpita, L. Jastrabik, P. Virostko, P. Adamek, P. Kudrna, S. Leshkov, M. Chichina, S. Kment, Langmuir probe diagnostics of a plasma jet system. Plasma Sources Sci. Technol. **18**(2009), 014009 (2009). https://doi.org/10.1088/0963-0252/18/1/014009
16. J. Olejnicek, J. Smid, R. Perekrestov, P. Ksirova, J. Rathousky, M. Kohout, M. Dvorakova, S. Kment, K. Jurek, M. Cada, Z. Hubicka, Co_3O_4 thin films prepared by hollow cathode discharge. Surf. Coat. Technol. **366**, 303 (2019). https://doi.org/10.1016/j.surfcoat.2019.03.010
17. J. Olejnicek, J. Smid, M. Cada, P. Ksirova, M. Kohout, R. Perekrestov, D. Tvarog, S. Kment, H. Kmentova, Z. Hubicka, High rate deposition of photoactive TiO_2 films by hot hollow cathode. Surf. Coat. Technol. **383**, 125256 (2020). https://doi.org/10.1016/j.surfcoat.2019.125256
18. G. Pribil, Z. Hubicka, R.J. Soukup, N.J. Ianno, Deposition of electronic quality amorphous silicon, a-Si:H, thin films by a hollow cathode plasma-jet reactive sputtering system. J. Vac. Sci. Technol. A **19**, 1571 (2001). https://doi.org/10.1116/1.1359537
19. Z. Hubicka, G. Pribil, R.J. Soukup, N.J. Ianno, Investigation of the rf and dc hollow cathode plasma-jet sputtering systems for the deposition of silicon thin films. Surf. Coat. Technol. **160**, 114 (2002)
20. R. Hippler, M. Cada, Z. Hubicka, A positively biased external anode for energy control of plasma ions: hollow cathode and magnetron sputtering discharge. Plasma Sources Sci. Technol. **30**, 045003 (2021). https://doi.org/10.1088/1361-6595/abe0cc
21. R. Hippler, M. Cada, V. Stranak, Z. Hubicka, C.A. Helm, Pressure dependence of Ar_2^+, $ArTi^+$, and Ti_2^+

dimer formation in a magnetron sputtering discharge. J. Phys. D Appl. Phys. **50**, 445205 (2017). https://doi.org/10.1088/1361-6463/aa8b9a
22. R. Hippler, M. Cada, V. Stranak, C.A. Helm, Z. Hubicka, Pressure dependence of singly and doubly charged ion formation in a HiPIMS discharge. J. Appl. Phys. **125**, 013301 (2019). https://doi.org/10.1063/1.5055356
23. S.H. Pullins, R.A. Dressler, R. Torrents, D. Gerlich, Z. Phys. Chem. **214**, 1279 (2000)
24. K. Okuno, Charge transfer of Ar^{2+} and Kr^{2+} in their own gases studied by the beam guide technique. J. Phys. Soc. Jpn. **55**, 1504 (1986)
25. T. Welzel, K. Ellmer, Negative oxygen ion formation in reactive magnetron sputtering processes for transparent conductive oxides. J. Vac. Sci. Technol. A **30**, 061306 (2012). https://doi.org/10.1116/1.4762815
26. A. Bogaerts, R. Gijbels, Role of Ar^{2+} and Ar_2^+ ions in a direct current argon glow discharge: a numerical description. J. Appl. Phys. **86**, 4124 (1999). https://doi.org/10.1063/1.371337
27. C. Paduraru, K.H. Becker, A. Belkind, J.L. Lopez, Y.A. Gonzalvo, Characterization of the remote plasma generated in a pulsed-DC gas-flow hollow-cathode discharge. IEEE Trans. Plasma Sci. **35**, 527 (2007). https://doi.org/10.1109/TPS.2007.895230
28. H. Deutsch, K. Becker, S. Matt, T.D. Märk, Theoretical determination of absolute electron-impact ionization cross sections of molecules. Int. J. Mass Spectrom. **197**, 37 (2000). https://doi.org/10.1016/S1387-3806(99)00257-2
29. H. Deutsch, P. Scheier, K. Becker, T.D. Märk, Revised high energy behavior of the Deutsch–Märk (DM) formula for the calculation of electron impact ionization cross sections of atoms. Int. J. Mass Spectrom. **233**, 13 (2004). https://doi.org/10.1016/j.ijms.2003.06.002
30. H. Deutsch, K. Becker, T.D. Märk, Calculated cross sections for the multiple ionization of nitrogen and argon atoms by electron impact. Plasma Phys. Control. Fusion **42**, 489 (2000). https://doi.org/10.1088/0741-3335/42/5/301
31. H. Deutsch, K. Becker, M. Probst, T.D. Märk, The semiempirical Deutsch-Maärk formalism: a versatile approach for the calculation of electron-impact ionization cross sections of atoms, molecules, ions, and clusters, in *Advances in Atomic, Molecular, and Optical Physics*, vol. 57, Chap 3 (Elsevier Inc., 2009), p. 87. https://doi.org/10.1016/S1049-250X(09)57003-6
32. D. Ascenzi, P. Franceschi, P. Tosi, D. Bassi, M. Kaczorowska, J.N. Harvey, Bond-forming reactions of dications: production of ArO^+ and ArO^{2+} in the reaction of Ar^{2+} with O_2. J. Chem. Phys. **118**, 2159 (2003). https://doi.org/10.1063/1.1533751
33. Atomic Spectra Database, NIST Standard Reference Database 78. https://doi.org/10.18434/T4W30F. Retrieved 11 August 2022
34. M.A. Lennon, K.L. Bell, H.B. Gilbody, J.G. Hughes, A.E. Kingston, M.J. Murray, F.J. Smith, Recommended data on the electron impact ionization of atoms and ions: Fluorine to nickel. J. Phys. Chem. Ref. Data **17**, 1285 (1988). https://doi.org/10.1063/1.555809